Suction caisson foundations for offshore wind turbines subjected to wave and earthquake loading: effect of soil–foundation interface

R. S. KOURKOULIS*, P. C. LEKKAKIS†, F. M. GELAGOTI* and A. M. KAYNIA‡

The response of wind turbines founded on suction caissons and subjected to lateral monotonic, cyclic and earthquake loading is studied with due consideration of the role of soil–sidewall adhesion, using non-linear three-dimensional finite-element analyses. In the case of monotonic and slow cyclic lateral loading it is shown that imperfect interface bonding could reduce the moment capacity and may lead to foundation detachment or even uplifting in the case of shallowly embedded caissons. A preliminary comparison of two caisson alternatives has shown that increasing the caisson diameter while maintaining the embedment ratio is more efficient in terms of material resources than increasing the skirt length while keeping the diameter constant. The second part of the study evaluates the response of a soil–foundation–wind turbine interacting system subjected to earthquake shaking. Contrary to an often prevailing impression that seismic effects are insignificant, apparently originating from evaluating the seismic behaviour on the basis of spectral characteristics, it is illustrated that the system kinematics may prove crucial for the response of large wind turbines subjected to simultaneous environmental and seismic loads. Although not instantly catastrophic, the accumulation of foundation rotation could lead to the turbine reaching serviceability limits early during its operation.

KEYWORDS: earthquakes; offshore engineering; soil/structure interaction

INTRODUCTION

Construction of off-shore wind-turbines of massive dimensions has recently become a major activity in the field of civil engineering as a result of European Union (EU) demands to produce 20% of its electricity by means of renewable energy sources by 2020. Uniquely, the foundation design of wind turbines is characterised by the challenging combination of relatively low weight and large horizontal loading due to the wind and wave currents, which produce large overturning moment at their bases (Houlsby & Byrne, 2000; Byrne & Houlsby, 2003).

Currently, several types of foundations are implemented for offshore wind turbines, depending on the site conditions and water depth. In waters of medium depth, the monopile option dominates the industry, with the alternative being a recently introduced scheme termed 'suction caisson', which was originally proposed for the foundation of off-shore oil platforms. It comprises a shallow footing whose capacity is enhanced by means of peripheral embedded skirts which confine the internal soil, thereby creating a soil plug. Ease of installation is the main advantage of this foundation type. The process consists of floating the caisson to its location, where it is driven into the seabed under the action of its self-weight and pumping of water trapped within the skirts. The differential pressure due to pumping creates suction which attracts the caisson lid downwards until it attains full contact with the soil.

Over the last decade, the design of skirted foundations and particularly suction caissons has been the subject of a significant amount of research (e.g. Bransby & Randolph, 1998; Andersen & Jostad, 1999; Randolph & House, 2002; Gourvenec & Randolph, 2003; Kelly *et al.*, 2006; Gourvenec, 2007; Bransby & Yun, 2009); these studies have offered valuable insight into the behaviour of such foundations. However, most of these results refer to foundations of limited skirt depth (low depth to diameter ratio, L/D) pertaining to off-shore oil platforms. As such, design of deeper caissons based on these results may be affected by the following uncertainties.

(*a*) Effect of soil non-uniformity: a widely used approach for accounting for soil profiles of linearly increasing strength is that proposed by Gourvenec & Randolph (2003) and Gourvenec (2007). It suggests, in principle, that the failure envelopes of a skirted foundation may be calculated on the basis of those of a shallow footing with equal dimensions resting at the skirt tip level of the original profile. This approach has been proven to provide correct failure envelopes when referring to shallow skirt embedment, but its accuracy reduces in the case of longer skirts (i.e. $L/D > 0{\cdot}2$) when the participation of the latter in sustaining the moment demand is much more significant. Indeed, centrifuge tests results by Tani & Craig (1995) and Watson & Randolph (1997) suggest this principle is reasonable for embedment depths less than around 30% of the foundation diameter.

(*b*) Effect of interface conditions: most studies on suction caisson foundations on clay tend to consider full contact between the foundation and the soil, in other words where the caisson can only detach from the surrounding soil if the strength of the latter is fully mobilised. This introduces two main assumptions, as follows.

(i) As a consequence of the installation method, the foundation is able to develop tensile capacity when the footing is subjected to uplift, owing to the negative excess pore pressures between the foundation lid and the confined soil. A series of experimental studies have been conducted to assess the

Manuscript received 23 November 2012; revised manuscript accepted 29 November 2013.
Discussion on this paper is welcomed by the editor.
* Laboratory of Soil Mechanics, National Technical University of Athens (NTUA), Greece.
† Stanford University, California, USA; formerly Laboratory of Soil Mechanics, NTUA, Greece.
‡ Norwegian Geotechnical Institute (NGI) and Norwegian University of Science and Technology (NTNU), Trondheim, Norway.

tensile capacity achieved by suction caissons (Clukey & Morrison, 1993; Colliat *et al.*, 1995; Mello *et al.*, 1998; Andersen & Jostad, 1999; Watson *et al.*, 2000; Houlsby *et al.*, 2005; Kelly *et al.*, 2006), showing that their tensile resistance may be comparable to their bearing capacity in compression, although this could depend on a number of factors (e.g. cavitation, rate of uplifting etc.).

(ii) Full contact is ensured between the skirts and the surrounding soil. Yet, experimental evidence has recently become available suggesting that this may not always be valid. House & Randolph (2001) conducted centrifuge tests on large L/D ratio suction caissons concluding to a friction ratio of 0·4 between the skirts and soil acting inside and outside the caisson. Andersen & Jostad (2002) suggest that an adhesion factor of 0·65 is applicable for a long period after the installation of suction anchors, while Jeanjean *et al.* (2006) have estimated a friction ratio of 0·85 at their interface. Gourvenec *et al.* (2009) experimentally measured a soil/skirt interface friction ratio as low as 0·3 during installation of low L/D ratios suction caissons; of course, these values refer to installation conditions in relatively lightly overconsolidated soil and are referenced here only as an indication of how low the friction ratio may potentially become.

(*c*) Load reference point: traditionally, the bearing capacity of embedded foundations subjected to combined loading is tackled by means of interaction diagrams produced by application of displacement on the base of the foundation. Yet, loading from wind turbines (stemming either from earthquake or simply from the wind, sea waves or currents) is transmitted from the turbine tower to the caisson top, and separation of the latter from the soil may modify the amount of loading imparted to its base.

(*d*) Response of wind turbines to earthquake: various studies on the seismic response of on-shore wind turbines (i.e. Bazeos *et al.*, 2002; Lavassas *et al.*, 2003; Ritschel *et al.*, 2003; Witcher, 2005; Haenler *et al.*, 2006; Zhao & Maisser, 2006), which were performed from a strictly structural engineering perspective, have highlighted the limited vulnerability of small-sized (i.e. 1 MW output or lower) wind turbines to earthquake. However, less attention has been given to the role of kinematic stressing transferred to the superstructure due to possible foundation displacement. This effect may become of significant importance when examining modern mega-sized turbines. Despite their dimensions (and hence large eigenperiods) these structures will, during the earthquake, be subjected to the concurrent unidirectional wind and current loading. This, although not disastrous (because wind turbine design codes impose very conservative limits to the maximum allowable rotation), could lead to the turbine reaching serviceability limits very early during its operation.

Based on this background, the scope of the current paper is to investigate the response of wind turbines founded on suction caissons subjected to monotonic lateral, cyclic and earthquake loading. Non-linear three-dimensional finite elements will be used in order to parametrically evaluate the effects of a linearly increasing strength profile and of soil–sidewall interfaces; emphasis will also be placed on the response of such structures to moderate and strong earthquake loading.

GEOMETRY AND MODELLING

The present research concerns offshore wind turbines founded on clay sites by suction caissons (Fig. 1). Depending on the parameter under investigation, two turbine assemblies (2 MW and 3·5 MW) were examined; their characteristics are displayed in Table 1. Both homogeneous and linearly increasing soil profiles were considered. In the former case a constant, undrained shear strength $s_u = 60$ kPa was assumed with Young's modulus $E_{stat} = 30$ MPa and $\nu = 0{\cdot}49$, whereas in the non-uniform deposit, the undrained shear strength s_{um} was assumed equal to 30 kPa at the seabed level and linearly increasing with depth with a gradient of $k = 3$ kPa/m. The undrained shear strength of $s_u = 60$ kPa corresponds to a relatively stiff clay formation allowing focus on the caisson response while avoiding exceptional soil yielding during the subsequent dynamic analyses. The soil has been assumed to be a single-phase material with submerged unit weight of $\gamma' = 10$ kN/m^3. The caisson diameter and embedment ratio was varied parametrically, as explained in the ensuing sections.

The problem is analysed using a three-dimensional (3D) finite-element (FE) model taking account of soil inelasticity. The developed FE model, taking advantage of problem

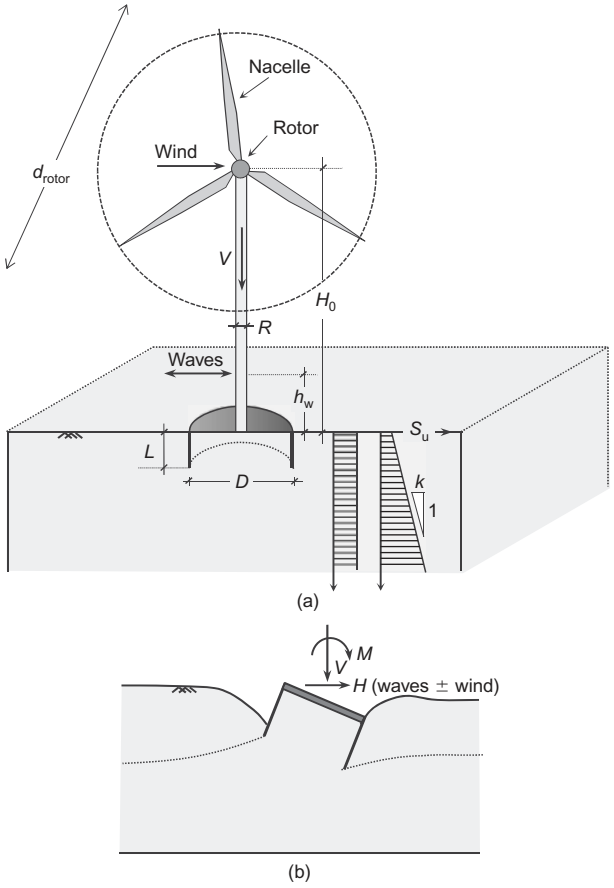

Fig. 1. (a) The problem under consideration and adopted notation: a wind turbine founded on suction caisson in either homogeneous or inhomogeneous soil, whose strength is linearly increasing with depth with gradient *k*. (b) Schematic diagram explaining the possibility of foundation detachment from surrounding soil when considering realistic shaft–soil interfaces

Table 1. Geometric properties of the examined wind turbines

	R: m	t: m	H_0: m	d_{rotor}: m	Nacelle + rotor mass: t_n
3·5 MW	2	0·023	80	90	220
2 MW	2	0·023	60	60	200

geometry symmetry, is displayed in Fig. 2. Soil is modelled with eight-noded hexahedral continuum elements. An initial sensitivity analysis revealed that the foundation diameter has to be discretised into at least 15 elements to effectively reproduce the mechanism of bearing capacity failure (due to vertical loading) as well as the mechanisms of soil yielding developed during its lateral loading.

Constitutive model

Non-linear soil behaviour is modelled through a simple kinematic hardening model with Von Mises failure criterion and associated flow rule, which is available in the Abaqus (2008) library and has been validated by Anastasopoulos *et al.* (2012) as to its capacity to simulate soil–structure interaction systems under cyclic or seismic loading. The model is appropriate for the simulation of clayey materials, the behaviour of which under undrained conditions may be considered as normal-pressure-independent. The evolution of stress is defined by

$$\sigma = \sigma|_0 + \lambda \tag{1}$$

where $\sigma|_0$ corresponds to the stress at zero plastic strain, and λ is a backstress parameter. The latter determines the kinematic evolution of the yield surface in the stress space through a function F where

$$F = f(\sigma - \lambda) - \sigma_0 \tag{2}$$

with $f(\sigma - \lambda)$ being the equivalent Mises stress with respect to the backstress α and σ_0 is the size of the yield surface. A one-dimensional representation of the non-linear stress low is provided in Fig. 3(a). At large plastic strains, when σ approaches σ_y, the magnitude of α becomes equal to $\alpha_s = E/\gamma_r$ and $(\sigma - \alpha)$ tends to σ_0 (Fig. 3), where E is the initial kinematic hardening modulus and γ_r is a parameter determining the rate of decrease of the kinematic hardening with increasing plastic deformation.

When considering clay materials, the maximum yield stress σ_y is controlled by the undrained shear strength of the material s_u as

$$\sigma_y = \sqrt{3} s_u \tag{3}$$

while

$$\sigma_0 = \sigma_y - \alpha_s = \sigma_y - E/\gamma_r \tag{4}$$

Therefore, for the full description of the constitutive model, only three parameters need to be determined: the strength s_u, the E/s_u ratio and the parameter γ_r. In other words, for a given s_u value, proper selection of the E/s_u ratio and the γ_r term allows for simulation of a wide range of materials of varying dynamic properties (G–γ and ξ–γ curves). Through the introduction of an external subroutine, the rate of increase of kinematic hardening may also be varied with respect to the level of plastic strain, which in turn offers additional versatility to the model.

The model adopted herein has been calibrated against measured data by Raptakis *et al.* (2000) referring to a clayey material of $s_u \approx 60$ kPa located at a depth of 10–20 m. Fig. 3(b) plots the result of the calibration procedure: the measured G–γ (shear stiffness–shear strain) and ξ–γ (damping–shear strain) curves are compared to those derived numerically by subjecting a soil element to cyclic simple shear loading at various amplitudes of strain γ.

Soil–foundation interfaces are simulated using special contact elements. The latter allow sliding and detachment arising from the tensionless interface behaviour. Such elements have been used in all vertical interfaces, that is between skirt and external and encaged (internal) soil. By appropriately adjusting the interface properties, it is possible to model a variety of contact conditions of practical interest ranging from the fully bonded to totally tensionless regime. Imperfect contact between the caisson and the sidewalls may be caused by a number of factors related either to the installation process (i.e. some amount of shearing during driving of the skirt) or to the multitude of loading cycles during the lifetime of a wind turbine, which could limit the available soil–foundation adhesion. In view of these, two assumptions have been made regarding the maximum shear resistance that may be offered at the soil–foundation interface: (*a*) $\alpha = 1$ corresponding to fully bonded interface

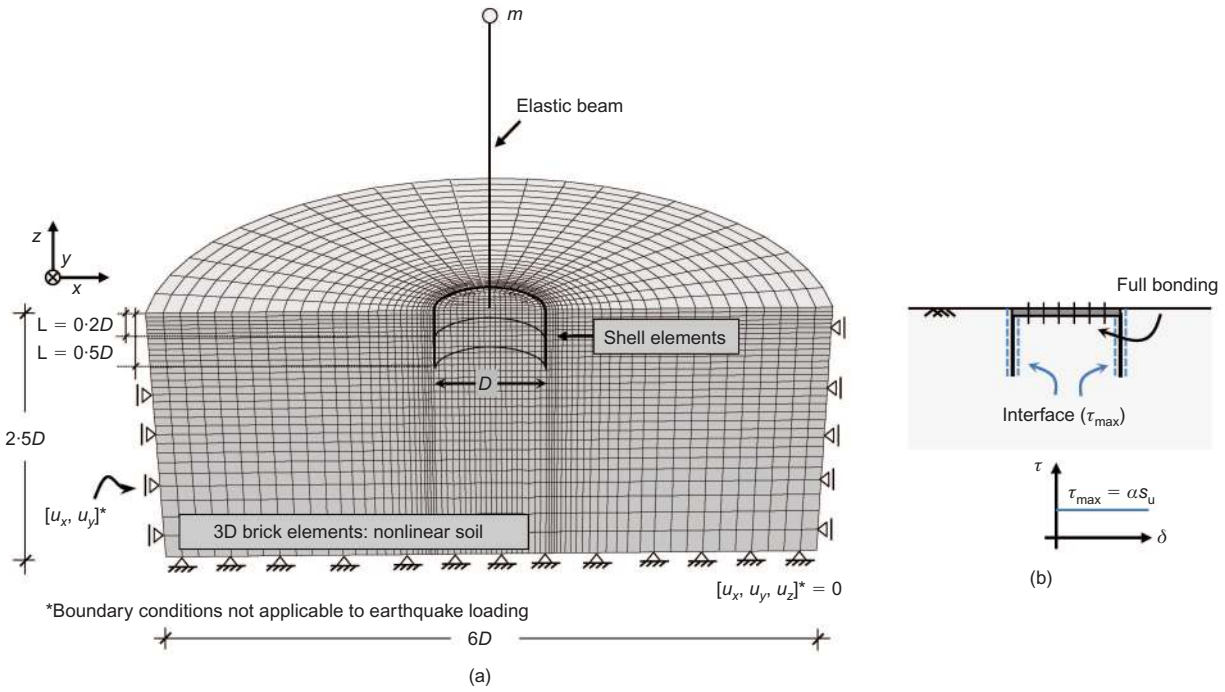

Fig. 2. (a) Finite-element mesh; (b) two assumptions are made for the caisson–soil interface: full adhesion ($\alpha = 1$) and reduced adhesion ($\alpha = 0{\cdot}3$)

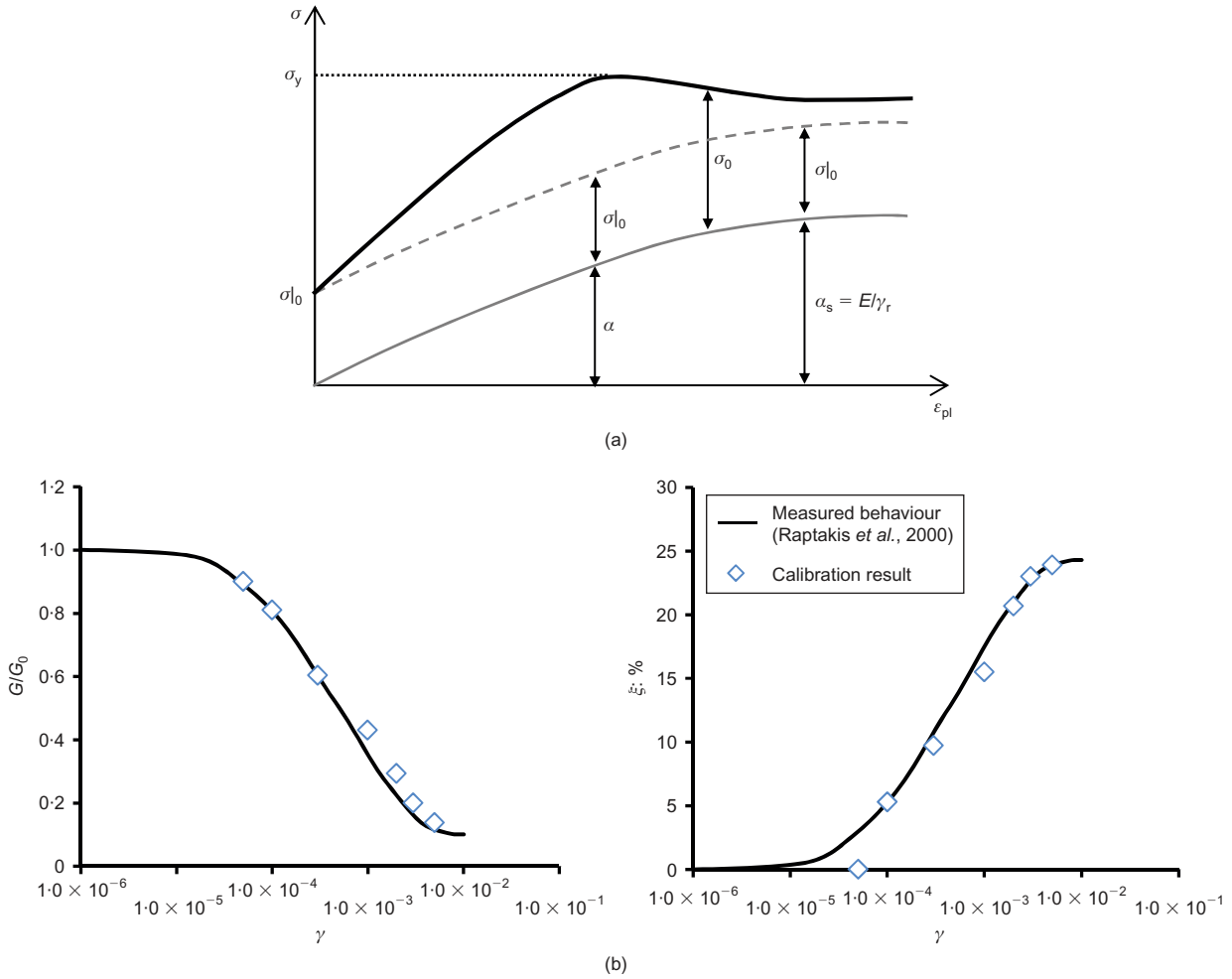

Fig. 3. (a) One-dimensional representation of the non-linear soil model. (b) Soil calibration result: each solid markers refers to the calculated G/G_0 ratio (or ξ%) when a single soil element is subjected to a cyclic simple shear test at a fixed strain amplitude, while the solid black line represents the target response

conditions or (b) $\alpha = 0{\cdot}3$ reflecting a significantly reduced adhesion at the interface, which has been deliberately chosen in order to more clearly demonstrate the potential effects of imperfect interface conditions. While it is also possible to model the contact conditions at the soil/caisson lid interface, it is assumed that the latter maintains perfect contact with the underlying soil, warranted by its tensile capacity as explained previously.

MONOTONIC LOADING: EFFECT OF SOIL INHOMOGENEITY AND INTERFACE CONDITIONS

An initial set of analyses is presented in this section which refers to displacement-controlled monotonic lateral loading applied at the centre of mass of the 3·5 MW turbine (assumed to lie at $H_c = 80$m from the caisson lid) until it attains its ultimate capacity, while considering the tower absolutely rigid so that focus is on the foundation response. Note that for the cases examined here, the combination of a very low V/V_{ult} (vertical load over vertical capacity) ratio with a very high lever arm (moment over horizontal force M/H) makes the moment capacity practically equal to that under pure moment loading M_0 under zero vertical loading ($V = 0$). Therefore, results of these sections are expected also to hold for taller wind turbines (e.g. 5 MW or 7 MW), as the ones currently implemented or planned. Results are plotted in terms of moment–rotation and settlement–rotation diagrams calculated on the base of the tower (i.e. foundation top) when the turbine is founded on a caisson with diameter $D = 20$ m. Two embedment depths with $L/D = 0{\cdot}2$ and $0{\cdot}5$ are compared, and the plots are presented in non-dimensional terms so as to maintain compatibility with the prevailing literature. However, attention is needed when comparing the results of uniform with non-uniform soil because the actual reference strength is different. To avoid misinterpretations, the actual shear strength $s_{u,0}$ at the skirt tip level for each case is highlighted on the diagrams.

Figure 4(a) compares the moment–rotation curves produced for the shallow caisson ($L/D = 0{\cdot}2$) in the homogeneous compared with the linearly increasing profile. When considering the uniform profile, it is evident that, despite their limited length, the skirts add significantly to the moment capacity, which reaches $M_{0{\cdot}2} = ADs_{u0}$. (where A is the caisson base surface), that is, an increase of the order of 50% compared to that of a surface foundation ($M_{sur} = 0{\cdot}67ADs_{u0}$). Yet, perhaps contrary to the reader's intuitive anticipation, consideration of linearly varying soil generates slightly higher moment capacity, despite its lower average strength along the skirt. (This holds true in non-dimensional terms; of course, the actual value of the moment capacity in the inhomogeneous soil case is lower than that of the uniform soil stratum.) Indeed, failure is governed by a scoop mechanism underneath the skirt, contained within soil of higher strength than that at the skirt tip level (s_{u0}), thus producing higher non-dimensional capacity.

Consideration of the reduced-adhesion scenario inevitably

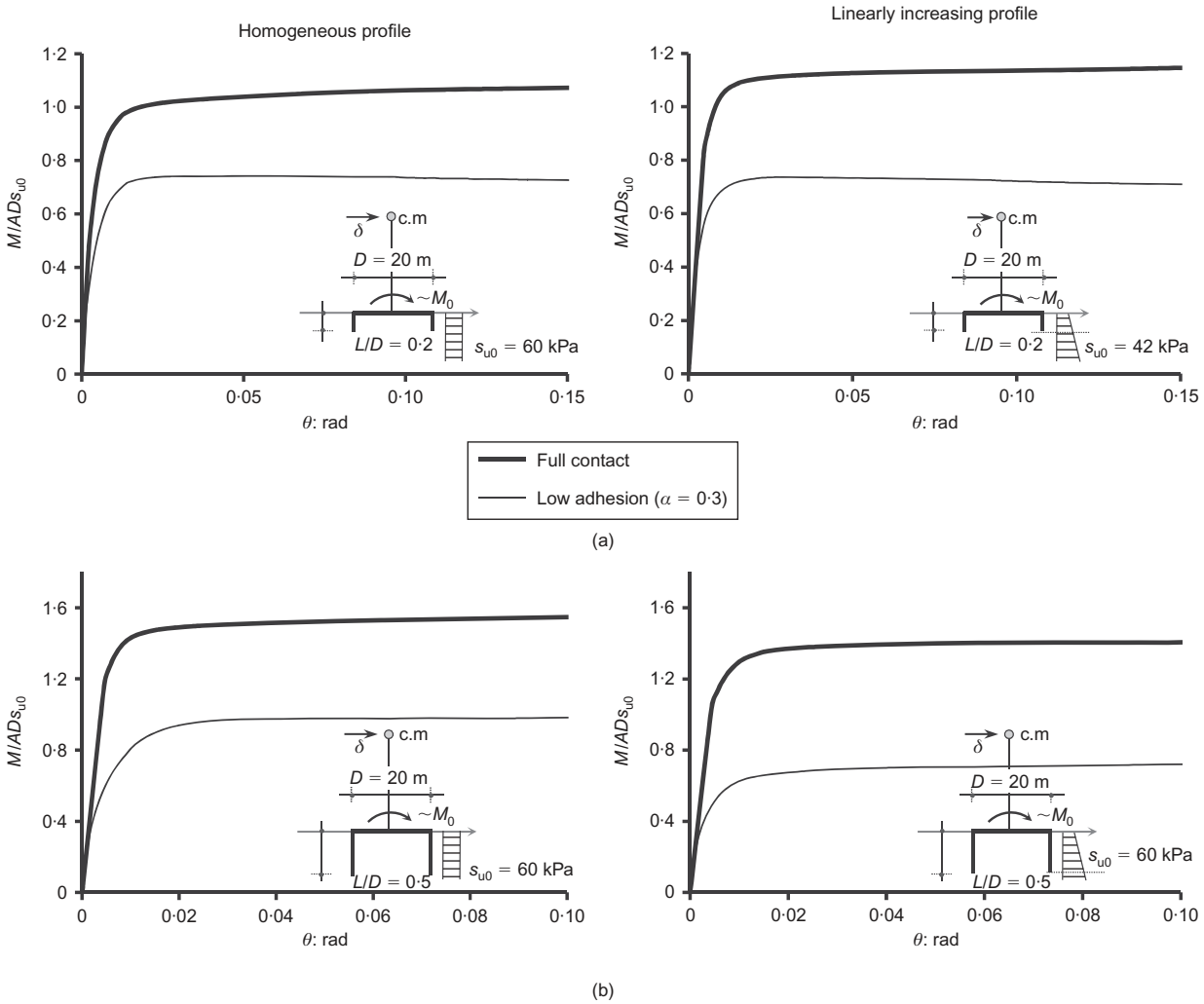

Fig. 4. Dimensionless moment–rotation curves obtained during monotonic lateral loading of the caisson in homogeneous and linearly increasing soil for the two interface scenarios: (a) shallow caisson: $D/B = 0{\cdot}2$, (b) deep caisson: $D/B = 0{\cdot}5$; c.m, centre of mass of the wind turbine

results in annulation of the shearing resistance offered by the part of the sidewalls opposite to the direction of displacement. As such, moment may be transmitted to the soil through the soil–lid interface (considered fully bonded throughout this paper) as well as the normal and shear stresses developed at the part of the skirt lying in the same direction as the loading, which is therefore unable to detach; naturally, this results in lower resistance than the scenario under full contact conditions.

The same pushover curves for the case of deeper embedment ($L/D = 0{\cdot}5$) are plotted in Fig. 4(b), reflecting the crucial role of the deeper sidewalls in offering resistance. The capacity of the deeply embedded caisson relies significantly on the contribution of the skirts, which apparently reduces as the adhesion factor decreases (leading to an overall capacity reduction by 40% for the homogeneous soil) while it drops dramatically when the lower adhesion is superimposed, with the skirts being contained within soil of reduced strength, as is the case of the linearly varying profile (where an overall capacity reduction by 65% is observed). Still, even when adopting the low-adhesion scenario, the dimensionless moment reaches a value which is higher than that of the surface foundation by almost 35% in the homogeneous profile.

The settlement–rotation curves of the two soil profiles are compared in Fig. 5. Notice that the initial static settlement (due to the weight of the structure) has been subtracted so that focus can be on the effect of lateral loading. Considering the full contact case (solid black lines) the graphs reveal that non-uniformity tends to limit the caisson's settlement independently of embedment depth.

To explain this behaviour the failure mechanisms are portrayed in Fig. 6. When the homogeneous profile is considered and full contact is ensured, the caisson internal soil system merges into one quasi-solid caisson whose reaction results in the formation of a deep scoop failure mechanism similar to the one identified by Bransby & Yun (2009). In the linearly varying profile (Fig. 6(b)), shear failure zones tend to form higher than in the uniform soil case due to the lower available strength in shallower strata. The nature of this profile generates partial mobilisation of the internal soil plug strength, thus producing an inverted scoop mechanism within the skirts in accord with findings by Yun & Bransby (2007), Bransby & Yun (2009) and Mana *et al.* (2010, 2013). The combination of a shallower external scoop, with the sliding of the foundation along the inverted internal scoop, limits the tendency of the foundation to settle, as evidenced in Fig. 5.

When the non-uniform profile is superimposed with the low adhesion interface (Fig. 6(c)), the very low sidewall resistance gives rise (in the extreme scenario examined) to sliding or even detachment of the caisson from the soil, thereby practically cancelling the formation of the external scoop, and may even result in foundation uplifting.

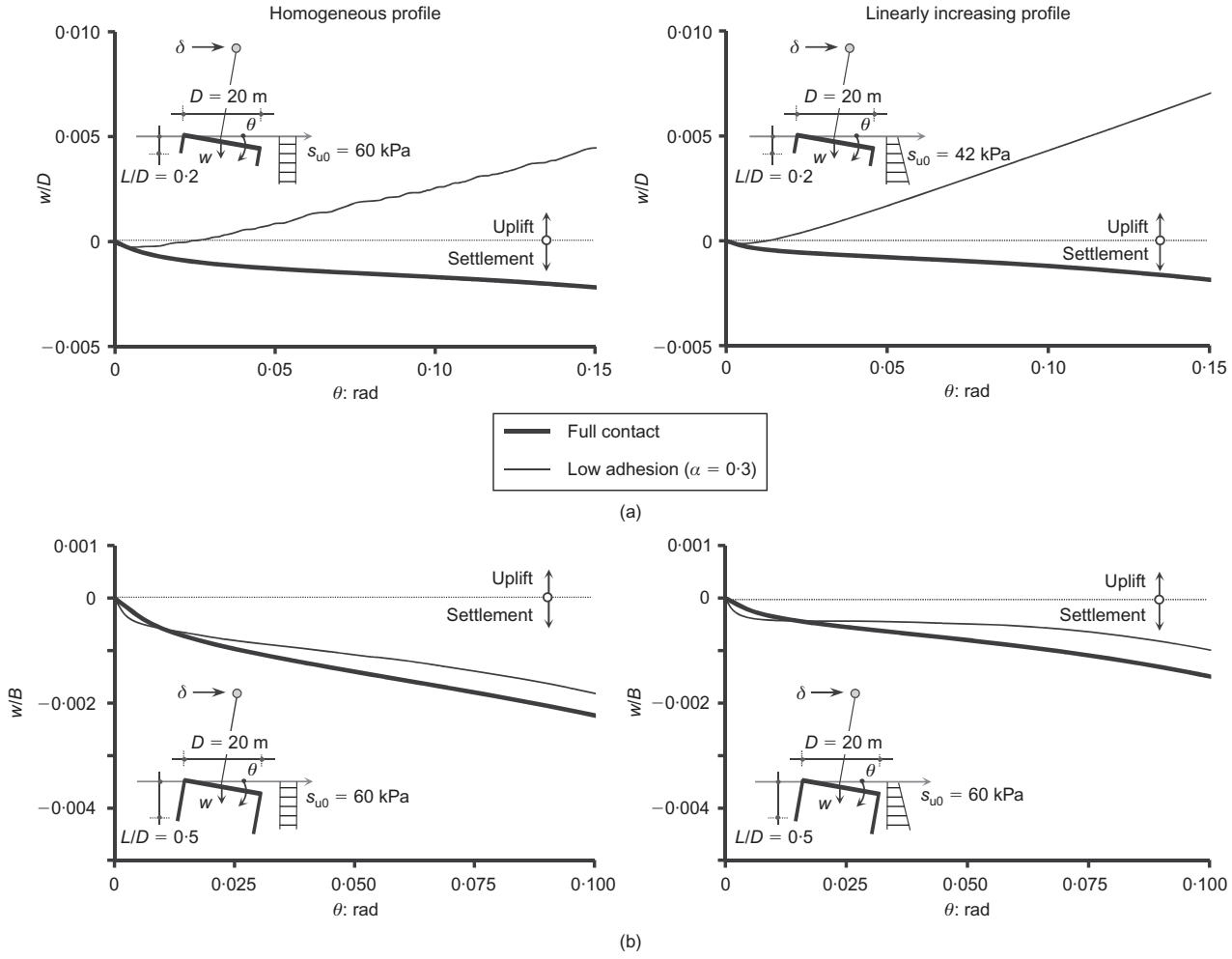

Fig. 5. Dimensionless settlement–rotation curves obtained during monotonic lateral loading of a caisson in homogeneous and linearly increasing soil for the two interface scenarios: (a) shallow caisson: $D/B = 0{\cdot}2$ (b) deep caisson: $D/B = 0{\cdot}5$

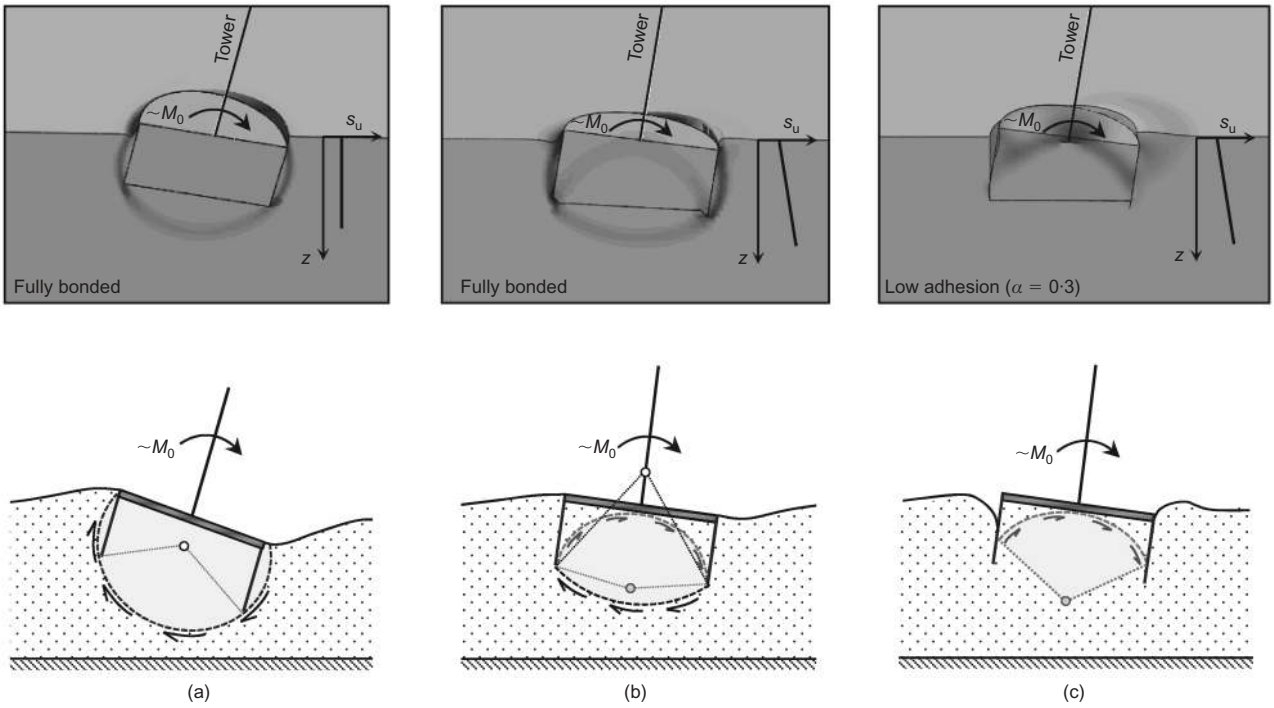

Fig. 6. Failure mechanism of a suction caisson of $L/D = 0{\cdot}5$ under (almost) pure moment loading (i.e. $H/H_{ult} \ll 1$, $V/V_{ult} \ll 1$): (a) homogeneous soil profile and fully bonded interface; (b) linearly increasing profile and fully bonded interface; (c) linearly increasing profile and low-adhesion interface

The results of non-linear foundation response are revisited in more detail in the next section, which examines the behaviour of the caisson subjected to cyclic loading.

CYCLIC LOADING: EFFECT OF IMPERFECT INTERFACE

In this section, the example caissons will be subjected to cyclic loading consisting of constant-amplitude displacement cycles, as explained below, attempting to derive a preliminary manifestation of the possible impact of earthquake loading. As such, they may serve as a preface for the ensuing dynamic analysis section. Again, the analyses presented in this section refer to displacement-controlled lateral loading cycles applied at the nacelle level of the 3·5 MW turbine (assumed to lie at $H_0 = 80$ m from the caisson lid), considering the tower as absolutely rigid and the caisson diameter $D = 20$ m.

Two sets of slow cyclic analyses were performed, each containing five equal-amplitude cycles. Both embedment ratios ($L/D = 0{\cdot}2$ and $0{\cdot}5$) and interface conditions were considered, while the soil was assumed homogeneous ($s_u = 60$ kPa). The first set (small cyclic loading) of analyses entailed application of displacements generating only minimal rotations of approximately 0·01 rad, which (according to the monotonic results) roughly correspond to the state of incipient soil yielding (Fig. 7, thin black line). The second set of analyses (large cyclic loading) consisted of imposing displacements that produced rotations of 0·05 rad (Fig. 7, bold black line), in order to stimulate excessive non-linearities and engender a yielding dominated response. Note that the unloading paths always obey Masing's principle – an inherent assumption of the adopted constitutive law.

The area of the loops (Fig. 7) indicates the energy dissipated during cyclic loading, which is dependent upon the amplitude of the imposed displacements. For the low-amplitude cycles, loops are quite negligible (nearly elastic behaviour). For the high-amplitude cycles, the loops tend to swell, echoing the inelastic response of the system and revealing the enhanced energy dissipation. Consideration of the low-adhesion interface tends to decrease energy dissipation, while in all cases the deeply embedded caisson offers substantially increased moment capacity compared to the shallow alternative. Note that in the full contact case (Fig. 7(a)), the diagrams follow the monotonic curve, which understandably is not the case when full contact is not warranted.

Figure 7(b) depicts the cyclic moment–rotation graphs for the 'low-adhesion' interface. For the low-amplitude cycles, the loops retain their original shape, owing to the fact that the system still remains approximately elastic and only minor separation between caisson and soil takes place. The difference is more conspicuous for the higher amplitude rotation of $\theta = 0{\cdot}05$, when the shape of the loop past the first cycle deviates from the monotonic curve and degenerates to a more pinched shape.

This is attributed to the effect of not only material non-linearities, but also geometric ones, manifesting themselves in the form of an irrecoverable gap behind the foundation (Fig. 8): as the caisson rotates during the first cycle towards one direction, it produces plastic deformation of the resisting soil (see point A), which may not be recovered once the direction of loading is reversed. Consequently, during the second cycle of loading towards the same direction, the existence of the gap reduces the overall resistance until the gap closes. Thus, the ability of the system to meet moment demands is severely weakened in between the extreme rotations, as evidenced by the flattened shape of the loop.

Naturally, in case of low L/D (Fig. 7(b)), even for the

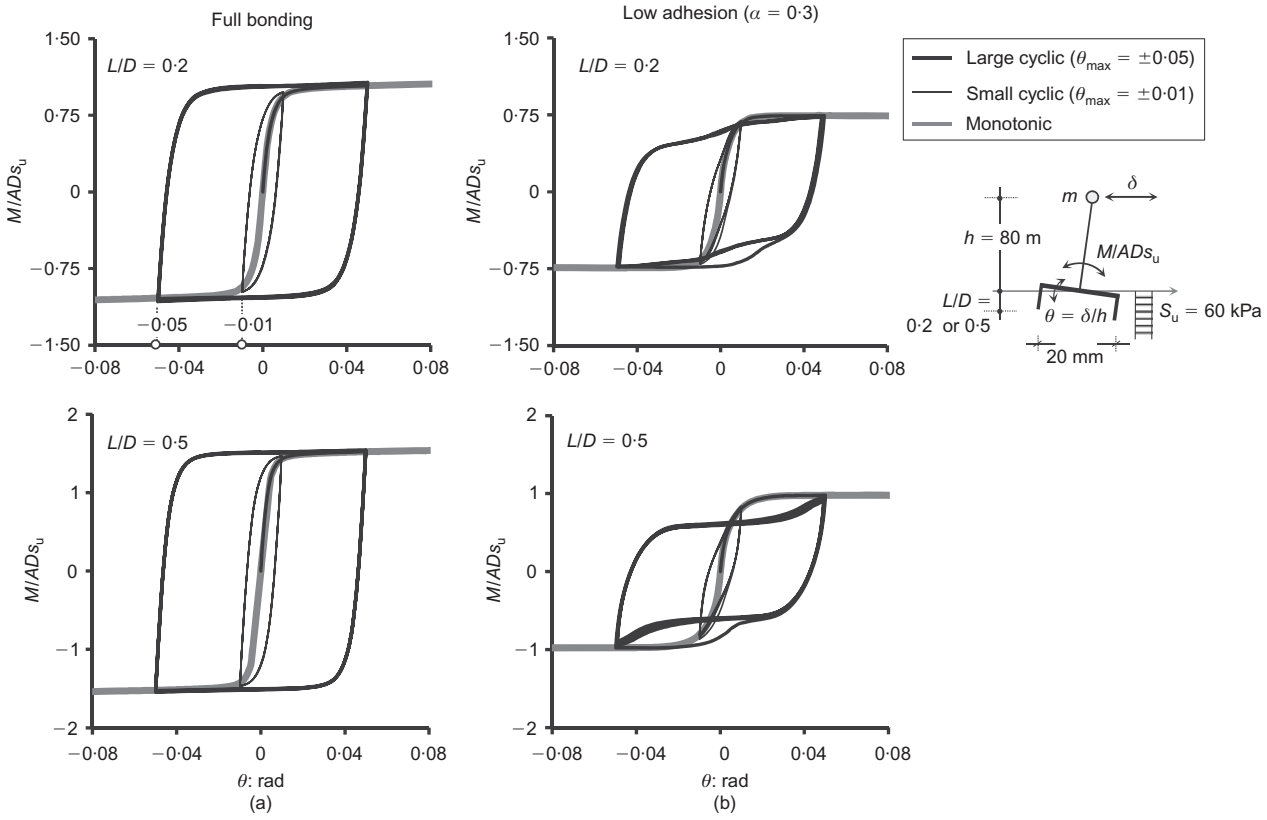

Fig. 7. Dimensionless moment–rotation loops obtained during slow cyclic lateral loading of the shallow ($L/D = 0{\cdot}2$, top) and the deeply ($L/D = 0{\cdot}5$, bottom) embedded caisson in homogeneous soil for the two interface scenarios: (a) full bonding; (b) low cohesion (numerical results refer to a 3·5 MW turbine ($H_0 = 80$ m) founded on a suction caisson with $D = 20$ m)

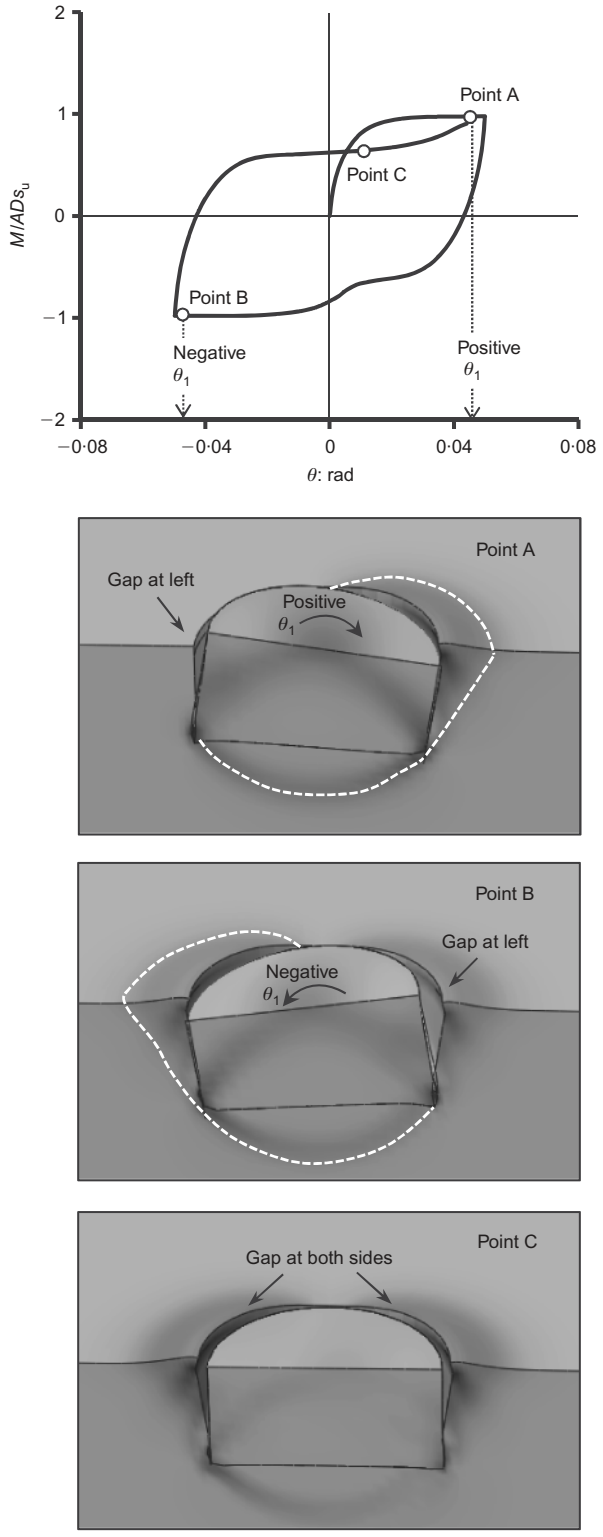

Fig. 8. Illustration of effect of detachment of caisson from surrounding soil on resulting moment–rotation loop

weak interface scenario, the shape of the M–θ loop is more rounded because the foundation response is controlled by the mobilised strength at the caisson base, while the lateral resistance and thus the possible formation of a gap cannot substantially modify the response in subsequent cycles of loading.

Quite similar conclusions may be drawn from the settlement–rotation diagrams (Fig. 9). Under the bonded interface regime (Fig. 9(a)) the initial settlement follows the monotonic curve, while it tends to progressively increase with the number of applied cycles of loading and mobilisation of more soil. Not surprisingly, for the high-amplitude cycles, excessive soil yielding is responsible for higher rotations and settlements. A marginally lower settlement is experienced by the $L/D = 0{\cdot}5$ caisson, which offers higher resistance.

The effect of low adhesion on the w–θ response is explored in Fig. 9(b). Again, for low-amplitude loading the response does not substantially differ from the full contact case: independently of embedment ratio, settlement keeps accumulating during each loading cycle. Discrepancies are much more pronounced with high-amplitude loading. For $L/D = 0{\cdot}2$, the diagrams for the 'low-adhesion' interface (Fig. 9(b)) indicate a rocking-dominated response of the caisson–soil system. Under the action of lateral loading, part of the foundation uplifts towards the loading direction while the pole of rotation instantaneously shifts towards its edge. Rocking of the foundation inevitably causes some soil yielding underneath it (due to the instantaneous reduction of its effective area), which results in the system finally experiencing some settlement during each loading–unloading–reloading cycle. Yet, the rate of accumulation of settlement remains remarkably lower than that under fully bonded conditions.

For the $L/D = 0{\cdot}5$ foundation (bottom plots), as discussed already, the larger area of the skirts provides increased resistance along the periphery and hence limits the uplifting ability of the caisson. Thus, settlement – due to soil yielding – keeps accumulating from the first cycle.

RESPONSE UNDER SERVICE LOADS: ROLE OF INTERFACES AND SOIL NON-UNIFORMITY

Having identified the mechanisms governing the response of suction caissons to displacement-controlled cyclic loading, this section is devoted to the behaviour of a typical 3·5 MW wind turbine on suction caissons to service loads. To better represent the loading conditions, the analyses were performed in force-controlled mode. The scope of this investigation is twofold

(*a*) to assess quantitatively the importance of interfaces and soil inhomogeneity
(*b*) preliminarily to weigh the balance of benefit between increasing the diameter D (while maintaining L/D constant) over increasing the depth of embedment (while keeping D constant).

The design of suction caissons was performed on the basis of loads acting on the turbine and allowable foundation rotation according to Houlsby & Byrne (2005). Three foundation configurations have been parametrically examined

(*a*) $D = 20$ m, $L/D = 0{\cdot}2$
(*b*) $D = 20$ m, $L/D = 0{\cdot}5$
(*c*) $D = 25$ m, $L/D = 0{\cdot}2$.

Apparently, the $D = 20$, $L/D = 0{\cdot}2$ set-up would be unacceptable but it is examined herein as an example of unconservative design; the remaining two alternatives may be considered as rational choices. Based on literature data (Table 1), the adopted amplitude values of wind and wave loads acting on the 3·5 MW turbine were taken as

(*a*) wind load: 1 MN, acting on the level of the rotor–nacelle assembly (80 m from mud-line)
(*b*) wave load: 1 ± 2 MN, acting on a height of approximately 7·8 m from the mud-line.

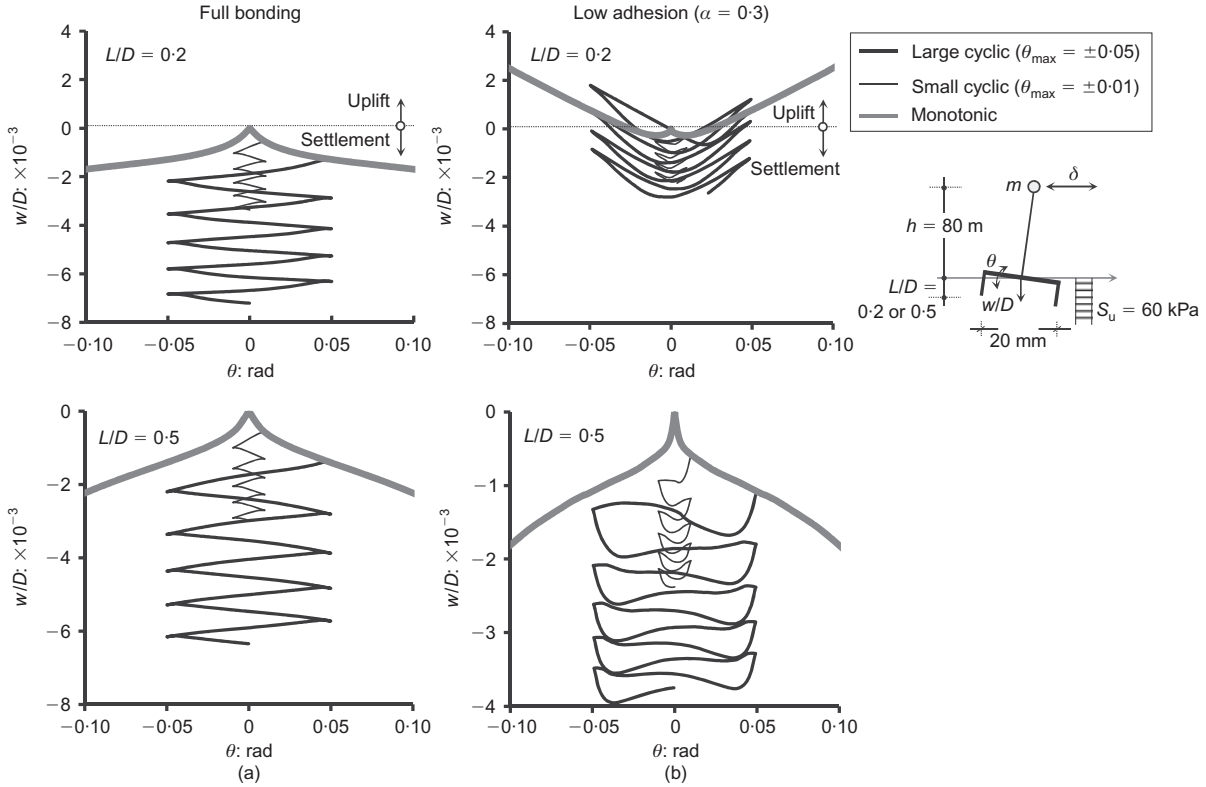

Fig. 9. Dimensionless settlement–rotation curves obtained during slow cyclic lateral loading of the shallow ($L/D = 0{\cdot}2$, top) and the deeply embedded ($L/D = 0{\cdot}5$, bottom) caisson in homogeneous soil for the two interface scenarios: (a) full bonding; (b) low adhesion ($\alpha = 0{\cdot}3$) (numerical results refer to a 3·5 MW turbine ($H_0 = 80$ m) founded on a suction caisson with $D = 20$ m)

Response to environmental loading

The first step of the analyses entailed the application of dead loads to the model. This was followed by a second loading step consisting of the application of wind load, modelled as a constant horizontal force on the level of the rotor, and a third step containing ten cycles of pseudo-statically imposed wave force.

In the ensuing analysis, serviceability capacity will be evaluated on the basis of current code limitations regarding the allowable deformations as follows

Settlement: $w_{max} = 0{\cdot}05B$, where B is the caisson diameter

Rotation: $\theta_{max} = 0{\cdot}001$ rad (DNV, 2001; Houlsby *et al.*, 2005).

Figure 10 plots the evolution of foundation rotation with increasing number of cycles for the cases examined. The same trends are in general observable in both the homogeneous and the linearly increasing profile, although rotations appear to be larger in the latter. Among the three types of foundations, the $B = 20$ m with $L/D = 0{\cdot}2$ clearly exhibits the largest values for rotation as well as incremental rotations, exceeding the serviceability rotation limit SL (despite the very limited number of loading cycles); a fact that, expectedly, renders it insufficient to support a typical 3·5 MW wind turbine. The remaining two caissons maintain almost constant rotation despite the increasing number of cycles. An interesting deduction is that by increasing the foundation's diameter while maintaining a low embedment ratio ($D = 25$ m, $L/D = 0{\cdot}2$), a more favourable response is achieved than by even substantially increasing the skirt length (i.e. from $L/D = 0{\cdot}2$ to $L/D = 0{\cdot}5$ in the $D = 20$ m case). Bearing in mind the fact that manufacturing of the two alternatives requires the same quantity of steel, it becomes evident that the former solution constitutes a more efficient foundation (assuming that the installation cost remains constant for both alternatives).

Consideration of the low-adhesion interface (Fig. 10(b)) produces augmented rotations in all cases, albeit the increase ratio is proportional to the original rotation value under full contact conditions, which means that the relative efficiency between the cases examined is preserved. The increase is about 45% for the $D = 25$ m footing, 57% for $D = 20$ m and $L/D = 0{\cdot}5$ and 68% for $D = 20$ m and $L/D = 0{\cdot}2$.

EARTHQUAKE LOADING

It is well known that construction of off-shore wind farms is being planned with increasing intensity worldwide, not excluding the seismically active regions (i.e. California, Japan, Italy and Greece). In general, wind turbines are low-frequency structures, and as such their structural systems are relatively insensitive to earthquake loading. Indeed, the first two eignefrequencies of the investigated 3·5 MW turbine have been numerically estimated at $f_0 = 0{\cdot}275$ Hz and $f_1 = 2{\cdot}75$ Hz respectively. These values agree with those analytically calculated following the Van der Tempel (2006) formula.

Understandably, these values will be even higher for larger turbines, as the ones currently planned (e.g. 5 MW), confirming the expectation for limited vulnerability of their structural systems to seismic loading. However, the focus of this section will be on the investigation of the soil–foundation–superstructure interaction, which may be responsible for additional kinematic loading being imposed on the system.

As already stated, the model turbines examined in this paper are assumed to be founded on an $s_u = 60$ kPa soil, corresponding to an intermediate category D soil according to the Eurocode 8 subsoil classification (CEN, 2004), which represents a layer of predominantly soft-to-firm cohesive soil. The imposed earthquake scenario will be typical of a moderate-to-strong seismicity region of Europe, correspond-

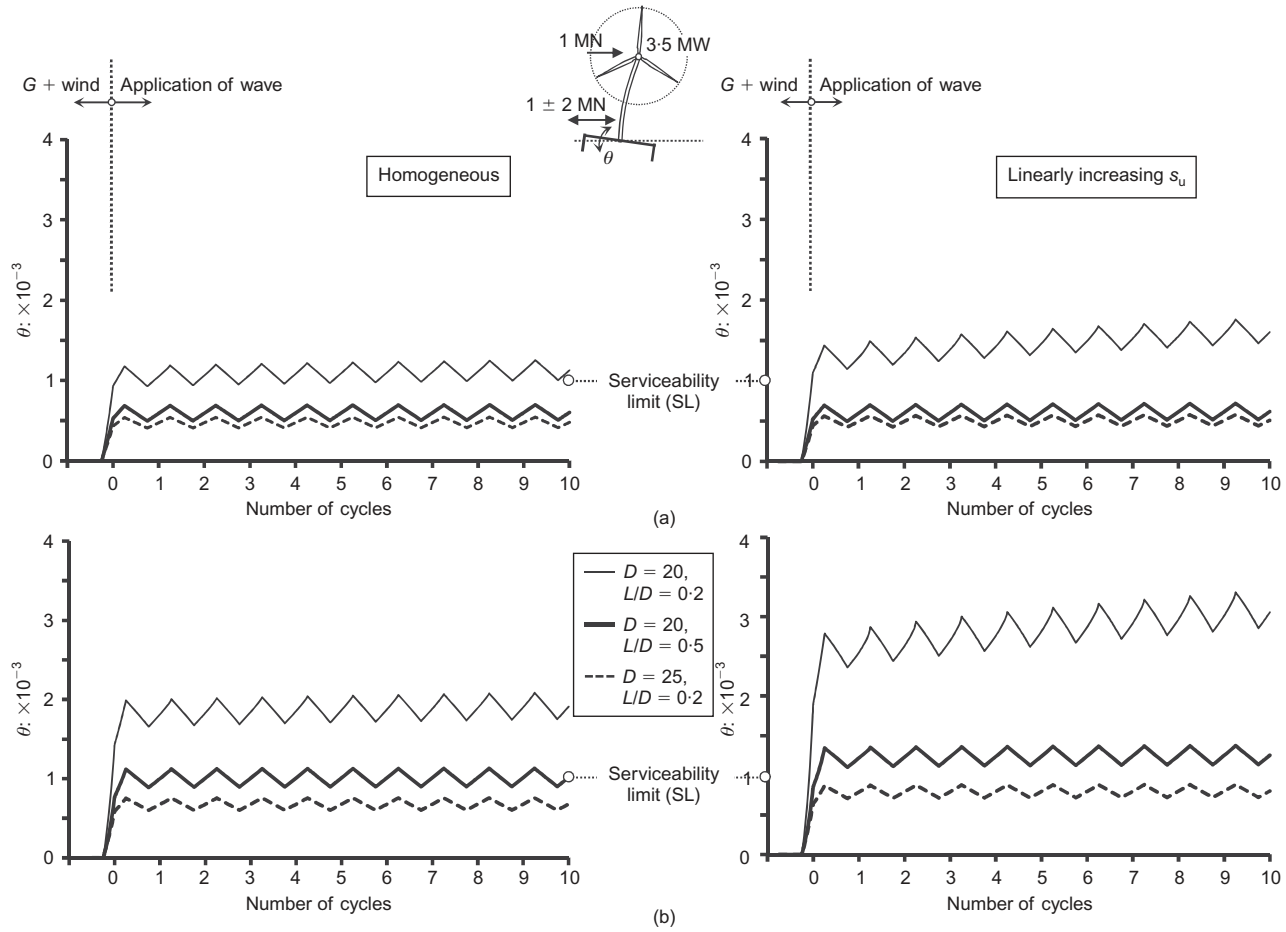

Fig. 10. Evolution of foundation rotation with increasing number of cycles of the 3·5 MW turbine foundation under environmental loads in both homogeneous and linearly increasing soil profiles assuming: (a) fully bonded interface; (b) low-adhesion interface

ing to a peak ground acceleration, PGA $= 0{\cdot}36\boldsymbol{g}$. The corresponding Eurocode 8 design spectrum is displayed in Fig. 11. The load combinations (i.e. of environmental and seismic loads) follow the norms set by the International Electrotechnical Commission (IEC) standard 61400/2005 (IEC, 2005) and are presented in Table 3.

The time histories applied to the base of the model are defined as modified Takatori and Rinaldi records (Fig. 11(a)) as they have originated after mathematically manipulating the Takatori and Rinaldi accelerograms recorded during the Kobe (Japan), 1995 and Northridge (USA), 1994 earthquakes respectively. As can be seen, the imposed spectral acceleration at the region of the dominant period ($T = 3{\cdot}6$ s) of the turbine is compatible with the Eurocode 8 spectrum for both scenarios examined.

The turbine is modelled as a 1-degree-of-freedom (dof) system consisting of a beam and a concentrated mass at the rotor–nacelle level. The beam section has been allocated the proper tower geometry and density so that the tower response is correctly represented. As such, the tower has been modelled as a steel pipe section of radius 2 m and thickness $t = 2{\cdot}3$ cm rendering a bending stiffness of EI ≈ 120 GNm^2.

The turbine has been assumed to be founded on the two foundation alternatives that are regarded as acceptable following the reasoning of the previous section: $D = 20$ m with $L/D = 0{\cdot}5$ and $D = 25$ m with $L/D = 0{\cdot}2$ (Fig. 11(c)). The initial elastic modulus over shear strength ratio, E_0/s_u, was taken as equal to 1800 following the calibration test presented previously. Proper kinematic constraints have been assumed at the lateral boundaries of the FE model to simulate free-field response (i.e. by creating a rigid disc at each level through the application of kinematic constraints between the node on the central axis and each peripheral node), while dashpot elements have been used at the base of the model to correctly reproduce radiation damping. The properties of the base 'substratum' are shown in Table 2. The damping coefficient of the dashpots is given by

$$C = \rho V_s A_d \tag{3}$$

where ρ is the material density, V_s the shear wave velocity and A_d the effective area of the dashpot (which depends on the mesh density at each region). A value of (Rayleigh) damping of $\xi_s = 3\%$ was adopted for the soil stratum in order to ensure viscoelastic response under even low strain amplitude. Based on the IEC 61400/2005 wind turbine design code the adopted tower damping was equal to $\xi_t = 1\%$.

Loading is again imposed in three steps. During the first step, the dead loads are applied to the model. This is followed by a second step consisting of the application of environmental loads, and a third dynamic step during which the time history analysis is conducted. Performance is assessed on the basis of the previously identified serviceability limit which, in terms of rotation, is $\theta_{max} = 0{\cdot}001$ rad.

Response to ground shaking

The acceleration–time histories recorded on the tower top are displayed in Fig. 12(a). Observe that, independently of the shaking scenario and the foundation type, the turbine response is maintained within controllable limits with the maximum experienced acceleration at $0{\cdot}25\boldsymbol{g}$. As anticipated, its oscillation is invariably out of phase with the excitation–

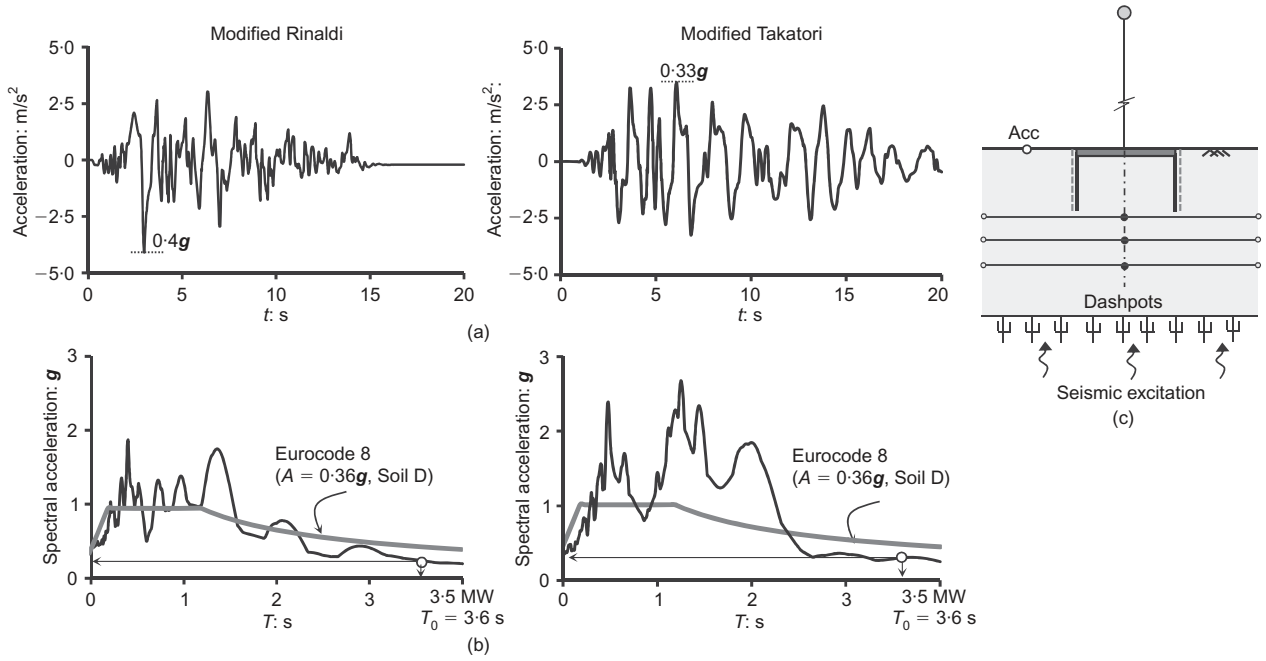

Fig. 11. (a,b) The modified Rinaldi and Takatori time histories used as input for the dynamic analyses along with their acceleration response spectra. (c) Boundary conditions allowing proper simulation of earthquake loading: dashpots at the bottom of the numerical model and kinematic constraints at the peripheral nodes

Table 2. Dashpot properties

s_u: kPa	E_0/s_u	ρ: t_n/m^3	V_s: m/s
120	1800	2	190

time history. The turbine oscillates mainly in its first eigenmode; yet excitation of its second mode is also evidenced by the 'curly' shape of the produced time histories. This intense vibration in small periods could cause dysfunction of the mechanical and electrical components of the rotor–nacelle assembly or affect the vibration of the blades.

The most interesting results, however, stem from the examination of the foundations' response. Both foundations offer quite large safety factors against overturning moment ($FS_M \approx 7$) and thus they are able to guarantee roughly equivalent fixity conditions on the tower base – a fact reflected in the tower's response. Consistently with this observation, the developed moments at the tower base (Fig. 12(b)) are practically the same for the two different embedment ratios. The fact that no significant discrepancy may be noticed between the two earthquake scenarios is primarily due to the large flexibility of the tower and is an additional indication of the limited sensitivity of the turbine to earthquake shaking.

Despite this observation, both foundations tend to accumulate rotation during each cycle, even during the mild modified Rinaldi shaking (Fig. 12(c)). Although a paradox according to initial spectral-based estimates, the long period of the 3·5 MW turbine is inadequate to render it insensitive to ground shaking when taking account of the whole foundation–structure system. On the contrary, the residual rotation may be increased to approximately six to seven times its initial value depending on the seismic scenario. This reveals a quite augmented detrimental effect of environmental (wind and wave) loading acting concurrently with the earthquake and hence producing unidirectional rotation, as explained in the next section and may be regarded as the direct analogue of a rigid body sliding along a slope.

Consistently with the conclusion drawn in the previous sections, consideration of the reduced-adhesion interface provokes a further 40–60% increase in rotation amplitude, although the experienced acceleration on the tower top as well as the general response pattern remain unchanged (Fig. 13).

Rotation build-up during each cycle is reasonably more intense in case of the more severe (modified Takatori) loading scenario, but does also takes place under the milder excitation scenario. Such accumulation of rotation is not directly threatening the safety of the structure, yet it constitutes irrecoverable damage to the serviceability of the turbine and might be responsible for curtailing the service life of the facility.

Table 3. Load and structure configuration combinations used in the earthquake loading analyses

	Foundation geometry		Loads		Foundation response	
	D: m	L/D	Wind: kN	Wave: kN	$\theta_0 \times 10^{-3}$	$M/M_{ult} = FS_M$
3·5 MW	20	0·5	1000	2000	0·26	7·0
	25	0·2			0·22	9·0
2 MW	17	0·2	350	1150	0·25	8·5

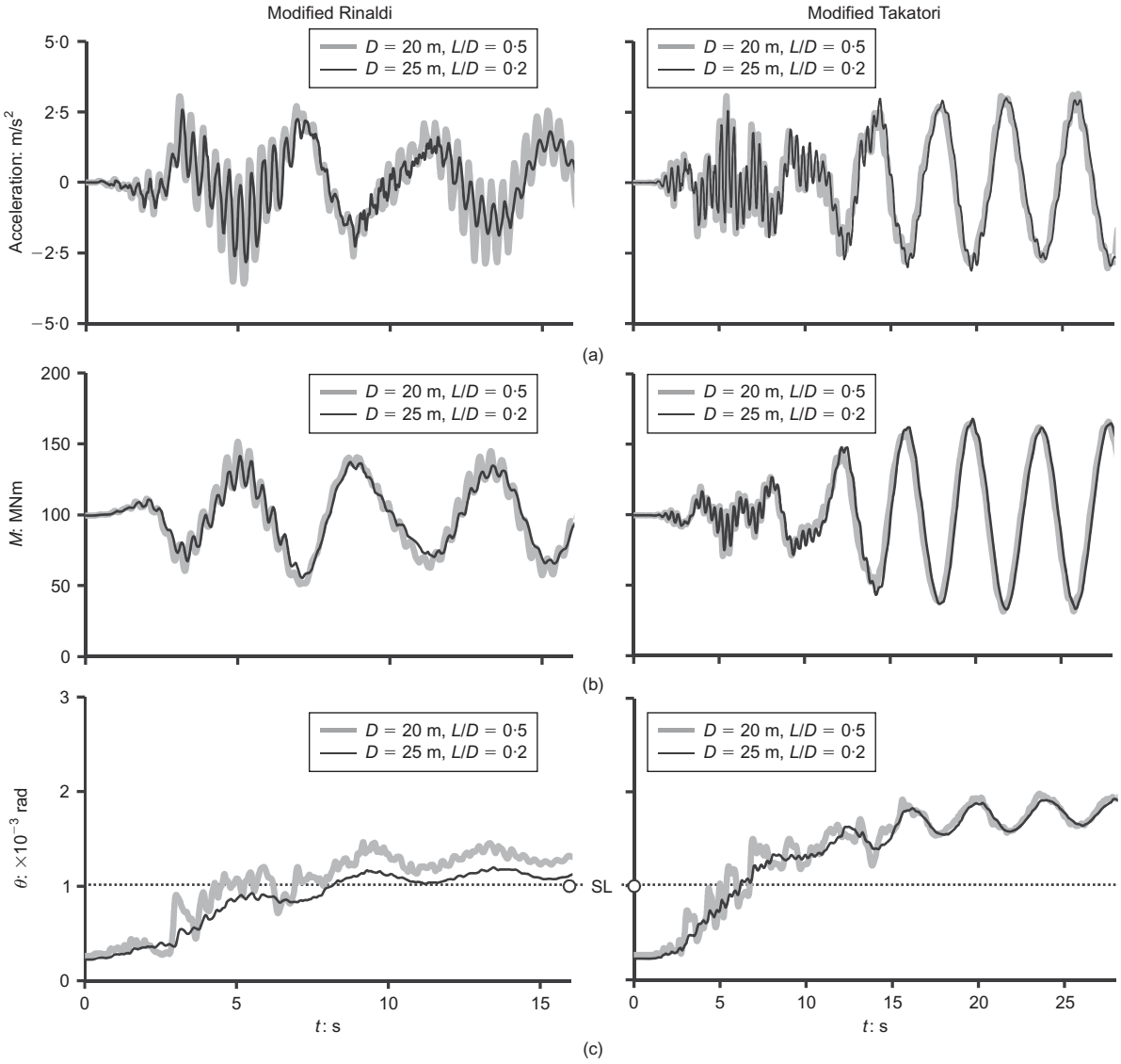

Fig. 12. Response of 3·5 MW turbine on the two foundation alternatives subjected to the two shaking scenarios assuming fully bonded conditions: (a) acceleration–time history at the tower top; (b) bending moment–time history at the tower base; (c) foundation rotation–time histories. The serviceability limit of $\theta = 1 \times 10^{-3}$ is marked on the diagrams

The role of inertial loading

Although already implied by the previous discussion, it is here attempted to unveil the potential fallacy of predicting the turbine seismic response based solely on spectral indications. To this end, Fig. 14 plots the rotation–time history on the foundation of the 3·5 MW turbine subjected to modified Rinaldi where the action of wind and waves are neglected. Noticeably, foundation rotation does take place; however, the rotation experienced during one cycle is recovered during the next, resulting in only negligible residual distortion – a response practically consistent with the anticipation engendered by examining the modified Rinaldi spectrum. In the same context, the figure also plots the response of a 2 MW superstructure whose higher eigenfrequencies ($f_0 = 0{\cdot}39$ Hz, $f_1 = 4{\cdot}75$ Hz) are expected to make it more prone to earthquake-induced distortion. In order to obtain comparable results with the 3·5 MW case, the 2 MW turbine is considered to be founded on a $D = 17$ m, $L/D = 0{\cdot}2$ foundation, which renders a safety factor against overturning moment, $\mathrm{FS}_{\mathrm{M}}^{2\,\mathrm{MW}} = 8{\cdot}5$ (recall $\mathrm{FS}_{\mathrm{M}}^{3.5\,\mathrm{MW}} = 9$). Its elastic rotation under the action of environmental loads is $\theta_0^{2\,\mathrm{MW}} = 2 \times 10^{-3}$, which is also very similar to that of the 3·5 MW turbine, thus rendering the two systems comparable under elastic conditions as well (Table 3). Indeed, the 2 MW tower, having higher natural frequencies, experiences significantly larger acceleration levels at its top. The most interesting results, however, once more appear when examining the foundation rotation plots (Fig. 14(b)). When neglecting environmental loads, the rotations experienced by the 2 MW foundation during shaking are larger than those of the 3·5 MW foundation. Yet, they are totally recoverable after the end of shaking. Observe that when considering the wind and current forces, the developed rotation is not only irrecoverable, but may exceed that of the 3·5 MW turbine. Remarkably, while the 2 MW foundation keeps accumulating rotation during each cycle, the foundation of the low-frequency 3·5 MW turbine acquires the most part of its residual rotation immediately after the strong pulse at about 6 s. This is a consequence of the substantially larger environmental loads acting on it, which compel the caisson to rotate although the structural vibration is practically insensitive to shaking.

Of course, significantly larger turbines are currently being planned or implemented than the ones examined herein; the greater flexibility of these is expected to result in limited vulnerability to seismic shaking. However, owing to their larger diameters, they are expected to carry greater concurrent

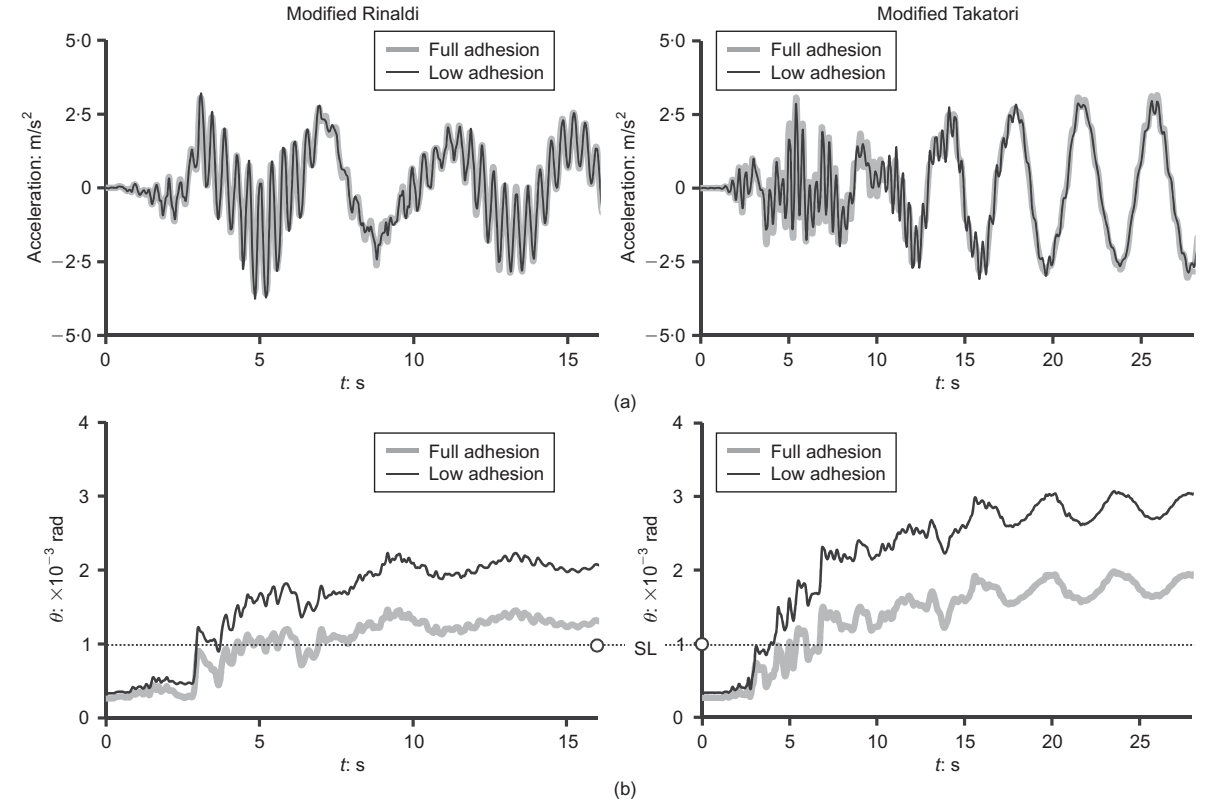

Fig. 13. Effect of cohesive interface on earthquake response of 3·5 MW turbine on the $D = 20$ m, $L/D = 0{\cdot}5$ caisson. Comparison of: (a) acceleration–time history at the tower top and (b) foundation rotation–time history assuming both perfect ($\alpha = 1$) and imperfect ($\alpha = 0{\cdot}3$) soil–foundation interface. SL, serviceability limit

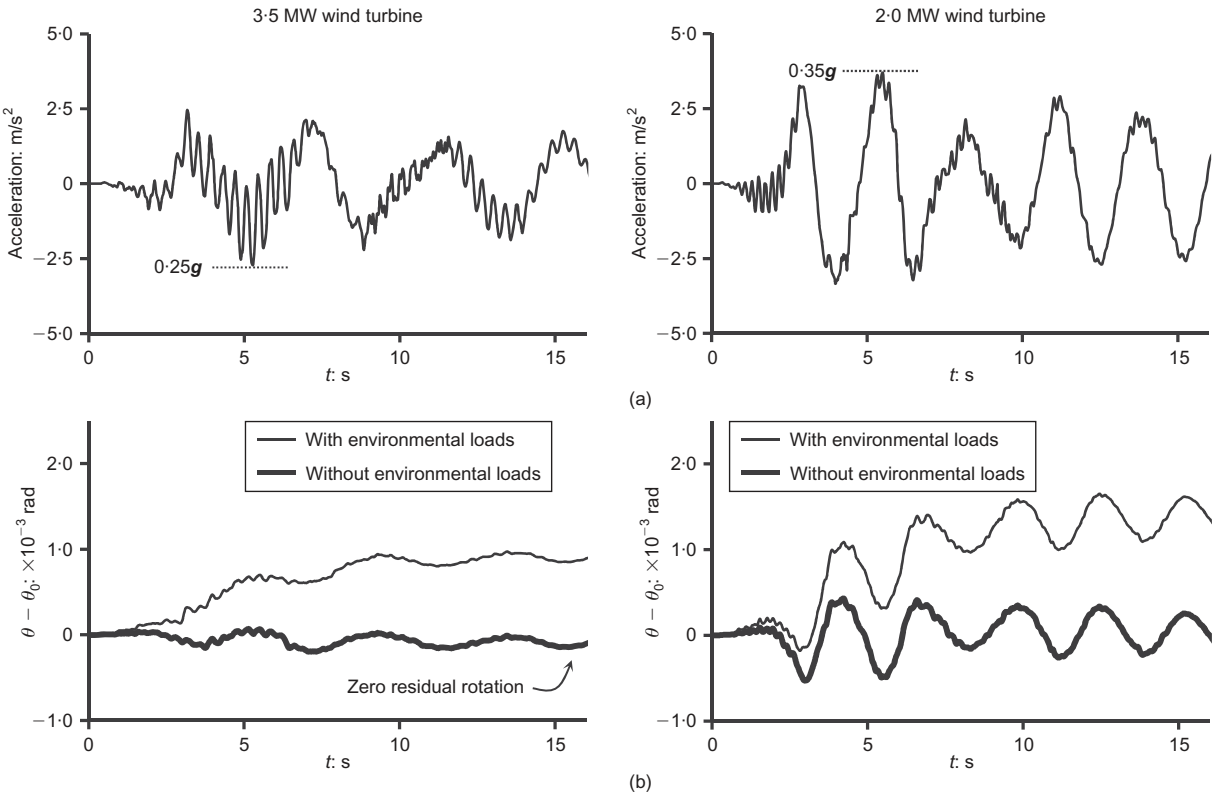

Fig. 14. Illustration of the role of unidirectional environmental loads for a 3·5 MW turbine (on a suction caisson with $D = 25$ m, $L/D = 0{\cdot}2$) and for a 2 MW turbine (on a caisson of $D = 17$ m and $L/D = 0{\cdot}2$): (a) acceleration–time history at the nacelle level of each turbine and (b) foundation rotation–time history. Both turbines are excited by the modified Rinaldi accelerogram

wind-induced moment that may prove important for the foundation performance.

CONCLUSIONS

This paper has investigated the response of a wind turbine founded on suction caissons subjected to monotonic lateral, cyclic and earthquake loading while parametrically investigating the role of soil–sidewall interface strength and soil non-uniformity. Consistent with previous studies, it was found that in the non-uniform profile, shear zones tend to form higher than in the uniform soil case, owing to the lower available strength in shallower strata, resulting in smaller settlements.

Consideration of imperfect interface conditions allows sliding or even detachment of the caisson from the soil, thus producing decreased foundation moment capacity. When considering a low-adhesion interface scenario, the lower shear resistance that may be offered on the peripheral sidewalls results in an inverted scoop mechanism mobilised within the skirts, thus producing larger plastic deformations and slightly increased settlements, even when deeply embedded caissons are considered. Under cyclic loading, the moment–rotation loops at high amplitudes of imposed displacement tend to develop a pinched shape due to gap formation. The low sidewall adhesion combined with its inadequate depth give rise to an uplifting-dominated response of the low L/D caisson when subjected to high amplitudes of displacement. On the other hand the deeply embedded $L/D = 0{\cdot}5$ caisson responds through accumulation of settlement.

A preliminary comparison of two caisson alternatives, each demanding the same amount of steel to manufacture, has shown that by increasing the foundation's diameter while maintaining a low embedment ratio ($D = 25$m, $L/D = 0{\cdot}2$), a more favourable response is achieved than by even substantially increasing the skirt length (i.e. from $L/D = 0{\cdot}2$ to $L/D = 0{\cdot}5$).

The response of the wind turbine to seismic shaking was assessed by subjecting it to a milder and a moderately strong earthquake scenario. It was shown that due to its large flexibility, the superstructure is generally insensitive to ground shaking. However, in terms of foundation response, the caisson tends to accumulate rotations during each loading cycle in both loading scenarios, resulting in significant residual rotation values. The latter may not be threatening the safety of the structure but constitute irrecoverable distortion that may question the serviceability of the turbine. Although limited in population and therefore inadequate to culminate in quantitative outcomes, the results of the analyses reveal the significance of properly accounting for earthquake loading combined with the environmental loads acting on the turbine: contrary to the misconception apparently originating from evaluating the seismic behaviour on the basis of inertial characteristics, it is proven that it is the system kinematics that ultimately govern the response.

ACKNOWLEDGEMENT

The financial support for this paper has been provided under the research project 'DARE', which is funded through the European Research Council's (ERC) 'IDEAS' Programme, in Support of Frontier Research – Advanced Grant, under contract/number ERC-2-9-AdG228254-DARE to Professor G. Gazetas.

NOTATION

A caisson base area
A_d effective area of dashpot
C damping coefficient of dashpots
D diameter of the caisson
d_{rotor} turbine diameter
E initial kinematic hardening modulus
E_{stat} Young's modulus under static loading
EI bending stiffness of steel pipe section in turbine tower model
F function
FS_M factor of safety against overturning moment
G shear stiffness
H/H_{ult} horizontal load over horizontal capacity
H_c height of centre of mass of turbine
H_0 height of the centre of mass of the nacelle measured from the seabed
k gradient of linearly increasing strength profile
L caisson length or depth of embedment
M/H moment over horizontal force ratio
R radius of the wind turbine tower
s_u undrained shear strength
s_{um} undrained shear strength at seabed level
$s_{u,0}$ shear strength at skirt tip level
T period of turbine
t thickness of steel pipe section in turbine tower model
t_n total mass of the nacelle and the rotor
V/V_{ult} vertical load over vertical capacity
V_s shear wave velocity
w_{max} settlement
α adhesion ratio
γ' submerged unit weight
γ_r parameter determining rate of decrease of kinematic hardening with increasing plastic deformation
θ foundation rotation
θ_{max} maximum rotation
θ_0 elastic rotation under action of environmental loads
λ backstress parameter
υ Poisson ratio
ξ hysteretic damping ratio
ξ_s value of (Rayleigh) damping for soil stratum
ξ_t adopted tower damping
σ normal stress
$\sigma|_0$ stress at zero plastic strain
σ_0 size of yield surface
σ_y maximum yield stress
ρ material density of dashpot

REFERENCES

Abaqus (2008). *ABAQUS: theory and analysis user's manual*, version 6.8-3. Providence, RI, USA: Dassault Systèmes Simulia Corp.

Abaqus (2010). *Standard user's manual*, Abaqus 6.10. Providence, RI, USA: Dassault Systèmes Simulia Corp.

Anastasopoulos, I., Gelagoti, F., Kourkoulis, R. & Gazetas, G. (2012). Simplified constitutive model for simulation of cyclic response of shallow foundations: Validation against laboratory tests. *J. Geotech. Geoenviron. Engng, ASCE* **137**, No. 12, 1154–1168.

Andersen, K. H. & Jostad, H. P. (1999). Foundation design of skirted foundations and anchors in clay. *Proceedings of the 31st offshore technology conference*, Houston, TX, paper OTC 10824.

Andersen, K. H. & Jostad, H. P. (2002). Shear strength along outside wall of suction anchors in clay after installation. *Proceedings of the 12th international offshore and polar engineering conference*, Kitakyushu, Japan. Mountain View, CA, USA: International Society of Offshore and Polar Engineers (ISOPE).

Bazeos, N., Hatzigeorgiou, G. D., Hondros, I. D., Karamaneas, H., Karabalis, D. L. & Beskos, D. E. (2002). Static, seismic and stability analyses of a prototype wind turbine steel tower. *Engng Structs* **24**, No. 8, 1015–1025.

Bransby, M. F. & Randolph, M. F. (1998). Combined loading of skirted foundations. *Géotechnique* **48**, No. 5, 637–655, http://dx.doi.org/10.1680/geot.1998.48.5.637.

Bransby, M. F. & Yun, G. J. (2009). The undrained capacity of skirted strip foundations under combined loading. *Géotechnique* **59**, No. 2, 115–125, http://dx.doi.org/10.1680/geot.2007.00098.

Byrne, B. W. & Houlsby, G. T. (2003). Foundations for offshore wind turbines. *Phil. Trans. R. Soc. London* **361**, No. 1813, 2909–2930.

CEN (Comité Européen de Normalisation) (2004). EN 1998-1: Eurocode 8: Design of structures for earthquake resistance – Part 1: General rules, seismic actions and rules for buildings. Brussels, Belgium: CEN.

Clukey, E. C. & Morrison, J. (1993). A centrifuge and analytical study to evaluate suction caissons for TLP applications in the Gulf of Mexico. In *Design and performance of deep foundations: Piles and piers in soil and soft rock*, ASCE Geotechnical Special Publication, vol. 38, pp. 141–156. Reston, VA, USA: American Society of Civil Engineers.

Colliat, J.-L., Boisard, P., Andersen, K. & Schroder, K. (1995). Caisson foundations as alternative anchors for permanent mooring of a Process Barge Offshore Congo. *Proceedings of the 27th offshore technology conference*, Houston, TX, paper OTC 7797, pp. 919–929.

DNV (Det Norske Veritas) (2001). *Guidelines for design of wind turbines*. Copenhagen, Denmark: Det Norske Veritas.

Gourvenec, S. (2007). Failure envelopes for offshore shallow foundations under general loading. *Géotechnique* **57**, No. 9, 715–728, http://dx.doi.org/10.1680/geot.2007.57.9.715.

Gourvenec, S. & Randolph, M. F. (2003). Effect of strength nonhomogeneity on the shape of failure envelopes for combined loading of strip and circular foundations on clay. *Géotechnique* **53**, No. 6, 575–586, http://dx.doi.org/10.1680/geot.2003.53.6.575.

Gourvenec, S., Acosta-Martinez, H. E. & Randolph, M. F. (2009). Experimental study of uplift resistance of shallow skirted foundations in clay under transient and sustained concentric loading. *Géotechnique* **59**, No. 6, 525–537, http://dx.doi.org/10.1680/geot.2007.00108.

Haenler, M., Ritschel, U. & Warnke, I. (2006). Systematic modelling of wind turbine dynamics and earthquake loads on wind turbines. *Proceedings of European wind energy conference and exhibition 2006, Athens, Greece*, pp. 1–6. Brussels, Belgium: European Wind Energy Association.

Houlsby, G. T. & Byrne, B. W. (2000). Suction caisson foundations for offshore wind turbines and anemometer masts. *Wind Engng* **24**, No. 4, 249–255.

Houlsby, G. T. & Byrne, B. W. (2005). Calculation procedures for installation of suction caissons in clay and other soils. *Proc. Instn Civil Engrs – Geotech. Engng* **158**, No. 2, 75–82.

Houlsby, G. T., Kelly, R. B., Huxtable, J. & Byrne, B. W. (2005). Field trials of suction caissons in clay for offshore wind turbine foundations. *Géotechnique* **55**, No. 4, 287–296, http://dx.doi.org/10.1680/geot.2005.55.4.287.

House, A. R. & Randolph, M. F. (2001). Installation and pull-out capacity of stiffened suction caissons in cohesive sediments. *Proceedings of the 11th international offshore and polar engineering conference*, Stavanger, Norway, vol. 2. Mountain View, CA, USA: International Society of Offshore and Polar Engineers (ISOPE).

IEC (International Electrotechnical Commission) (2005). IEC 61400-1: Wind turbines – Part 1: design requirements. Geneva, Switzerland: IEC.

Jeanjean, P., Znidarcic, D., Phillips, R., Ko, H.-Y., Pfister, S., Cinicioglu, O., & Schroeder, K. (2006). Centrifuge testing on suction anchors: double-wall, over-consolidated clay, and layered soil profile. *Proceedings of the offshore technology conference*, Houston, TX, paper OTC 18007.

Kelly, R. B., Houlsby, G. T. & Byrne, B. W. (2006). Transient vertical loading of model suction caissons in a pressure chamber. *Géotechnique* **56**, No. 10, 665–675, http://dx.doi.org/10.1680/geot.2006.56.10.665.

Lavassas, I., Nikolaidis, G., Zervas, P., Efthimiou, E., Doudoumis, I. N. & Baniotopoulos, C. C. (2003). Analysis and design of the prototype of a steel 1-MW wind turbine tower. *Engng Structs* **25**, No. 8, 1097–1106.

Mana, D. S. K., Gourvenec, S. & Randolph, M. F. (2010). A numerical study of the vertical bearing capacity of skirted foundations. *Proceedings of the 2nd international symposium on frontiers in offshore geotechnics (ISFOG)*, Perth, pp. 433–438.

Mana, D., Gourvenec, S. & Martin, C. (2013). Critical skirt spacing for shallow foundations under general loading. *J. Geotech. Geoenviron. Engng, ASCE* **139**, No. 9, 1554–1566.

Mello, J. R. C., Moretti, M. J., Sparrevik, P., Schroder, K. & Hansen, S. B. (1998). PI9 and P26 moorings at the Marlim field. The first permanent taut leg mooring with fibre rope and suction anchors. *Proceedings of the FPS '98 conference*, London, UK, P19.

Randolph, M. F. & House, A. R. (2002). Analysis of suction caisson capacity on clay. *Proceedings of the annual offshore technology conference*, Houston, TX, paper OTC 14236.

Raptakis, D., Chávez-García, F. J., Makra, K. & Pitilakis, K. (2000). Site effects at EUROSEISTEST Part I. Determination of the valley structure and confrontation of observations with 1D analysis. *Soil Dynam. Earthquake Engng* **19**, No. 1, 1–22.

Ritschel, U., Warnke, I., Kirchner, J. & Meussen, B. (2003). Wind turbines and earthquakes. *Proceedings of the 2nd world wind energy conference, Cape Town, South Africa*. Bonn, Germany: World Wind Energy Association (CD-ROM).

Tani, K. & Craig, W. H. (1995). Bearing capacity of circular foundations on soft clay of strength increasing with depth. *Soils Found*. **35**, No. 2, 37–47.

Van der Tempel, J. (2006). *Design of support structures for offshore wind turbines*. PhD thesis, Delft University of Technology, Delft, the Netherlands.

Watson, P. G. & Randolph, M. F. (1997). Vertical capacity of caisson foundations in calcareous sediments. *Proceedings of the 7th international offshore and polar engineering conference*, Honolulu, vol. 1, pp. 784–790. Mountain View, CA, USA: International Society of Offshore and Polar Engineers (ISOPE).

Watson, P. G., Randolph, M. F. & Bransby, M. F. (2000). Combined lateral and vertical loading of caisson foundations. *Proceedings of the offshore technology conference*, Houston, TX, paper OTC 12195.

Witcher, D. (2005). Seismic analysis of wind turbines in the time domain. *Wind Energy* **8**, No. 1, 81–91.

Yun, G. & Bransby, M. F. (2007). The undrained vertical bearing capacity of skirted foundations. *Soils Found*. **47**, No. 3, 493–505.

Zhao, X. & Maisser, P. (2006). Seismic response analysis of wind turbine towers including soil–structure interaction. *Proc. Instn Mech. Engrs, Part K: J. Multi-Body Dynam*. **220**, No. 1, 53–61.